Ice and water permittivities for millimeter and sub-millimeter remote sensing applications

Jonathan H. Jiang* and Dong L. Wu

Jet Propulsion Laboratory, California Institute of Technology, Pasadena, California, USA

*Correspondence to:
Jonathan H. Jiang, Jet Propulsion
Laboratory, California Institute of
Technology, Pasadena,
California, USA.
E-mail:
Jonathan.H.Jiang@jpl.nasa.gov*

Abstract

Recent advances in satellite remote sensing at near-millimeter and sub-millimeter wavelengths ($\sim$100–3000 GHz) require accurate complex permittivity for ice and liquid water at these frequencies for different temperatures, especially for cold atmospheric conditions. This paper summarizes the existing experimental permittivity data in the literature and provides an updated empirical ice permittivity model for radiative transfer calculations for ground and space remote sensing experiments. Applications of this permittivity model to Microwave Limb Sounder (MLS) cloud measurements are discussed. Copyright © 2004 Royal Meteorological Society

Keywords: cloud ice and water; microwave remote sensing; complex permittivity

1. Introduction

Modeling cloud radiative properties requires accurate knowledge of the relative refractive index $m = m_1/m_o$ of ice and water hydrometers, where $m_1 = n' - in''$ is a complex refractive index and m_o is the index of the surrounding medium. For the Earth's atmosphere, $m_0 = 1$, and m is simply equal to the particle refractive index, which is the square root of the complex dielectric permittivity ε,

$$m = \sqrt{\varepsilon} \tag{1}$$

where

$$\varepsilon = \varepsilon' - i\varepsilon''. \tag{2}$$

The real part of the permittivity, ε', the dielectric constant, is a parameter to describe how the electric field polarizes matter; the imaginary part, ε'', or loss factor, describes how electromagnetic waves are absorbed.

The dielectric properties (ε', ε'') of ice and water hydrometeors suspended in clouds play a key role in computing the radiative transfer under cloudy sky conditions, which can affect microwave propagation in the atmosphere. For the Microwave Limb Sounder (MLS) cloud measurements, we developed an empirical model based on the parameterizations in Liebe *et al.* (1989, 1991) and Hufford (1991) (hereafter the LH model). The LH model was developed using empirical fits to published experimental data at frequencies < 1000 GHz for both ice and water, and limited to temperatures $\geq 0\,°C$ for water. The Earth Observing System (EOS) MLS instrument (which was launched onboard the EOS Aura Satellite on 15 July, 2004) carries radiometers with frequencies up to 2500 GHz, most of which measure the atmosphere

at very low temperatures ($<0\,°C$). Therefore, permittivity models of ice and liquid water over a broader frequency interval are needed, especially for the imaginary part of the permittivity of ice at high frequencies (600–2500 GHz).

In this paper, we extend the original LH dielectric permittivity (ε', ε'') model for pure ice to frequencies up to 3000 GHz and compare the updated parameterizations of ice and water permittivity to laboratory measurements reported in the literature. Applications of this extended model to Mie calculations and uncertainties at EOS MLS frequencies are discussed.

2. The complex permittivity for pure ice and water

For pure-water ice, the original LH model formulates the complex permittivity by

$$\varepsilon'_{ice} = 3.15$$
$$\varepsilon''_{ice} = \alpha(T)/\nu + \beta(T)\nu \tag{3}$$

where ν is frequency in GHz, and $\alpha(T)$ and $\beta(T)$ are temperature-dependent parameters fitted to laboratory measurements (Hufford, 1991). For pure liquid water, the formulations are

$$\varepsilon'_{water} = (\varepsilon_0 - 5.48)/[1 + (\nu/\nu_P)^2]$$
$$+ 1.97/[1 + (\nu/\nu_S)^2] + 3.51$$
$$\varepsilon''_{water} = (\varepsilon_0 - 5.48)(\nu/\nu_P)/[1 + (\nu/\nu_P)^2]$$
$$+ 1.97(\nu/\nu_S)/[1 + (\nu/\nu_S)^2] \tag{4}$$

where ε_0, ν_P and ν_S are all temperature-dependent parameters (Liebe *et al.*, 1991).

To extend the LH formulae to frequencies >1000 GHz, we modified the LH expression for the imaginary part of the dielectric permittivity of ice by including a ν^3 term in Equation (3), based on the far-infrared work by Mishima *et al*. (1983), namely,

$$\varepsilon''_{\text{ice}} = \alpha(T)/\nu + \beta(T)\nu + \gamma\nu^3, \qquad (5)$$

where γ can be calculated from the B factor in Equation(16) in Mishima *et al*. (1983) via the following. The additional B dependent absorption K_a can be expressed as twice the attenuation coefficient α (Ulaby *et al*., 1981), i.e.

$$K_a = 2\alpha = \frac{2\pi}{c}f|Im\{\varepsilon\}| = \frac{2\pi}{c}f\frac{\varepsilon''}{\sqrt{\varepsilon'}} = B\left(\frac{f}{c}\right)^4, \qquad (6)$$

where c is the speed of light in units of cm/s, f is frequency in units of Hz, factor $B = 1.11 \times 10^{-6}$ cm^{-4} is given by Mishima *et al*. (1983). Rearranging Equation (6), we obtain an expression for the additional ν^3 dependent permittivity ε'':

$$\varepsilon'' = \sqrt{\varepsilon'}\frac{B}{2\pi c^3}f^3 = 10^{27}\sqrt{\varepsilon'}\frac{B}{2\pi c^3}\nu^3 = \gamma\nu^3. \qquad (7)$$

The factor 10^{27} is the result of changing the frequency expression from f (in Hz) to ν (in GHz). Substituting the values of B and c, one obtains $\gamma = 10^{27}(\varepsilon')^{1/2}B/(2\pi c^3) = 1.16 \times 10^{-11}$.

For the real part of the ice permittivity, we assume the LH formula stays the same at higher frequencies, as do the real and imaginary parts of the permittivity of water.

3. Comparisons to laboratory measurements

3.1. The permittivity of pure ice

Laboratory measurements of the imaginary part of the ice refractive index or dielectric permittivity have been made and published by a number of researchers at millimeter and sub-millimeter wavelengths; they are summarized in Figure 1 with comparison to the modified LH model (Equation (5)). The solid lines in Figure 1 show the imaginary ice dielectric permittivity computed by the modified LH model at different temperatures. The dotted lines are the original curves computed from the original LH formula (Equation (3)). The measured data are described in the following.

Mätzler and Wegmüller (1987) presented measurements for the coefficient β at temperatures between 0 and $-30\,°$C. The values of their ε'' at $-3\,°$C and $-10\,°$C in Figure 1 are estimated by using the modified LH formula. Note, however, *Mätzler and Wegmüller*'s β is slightly different from the β we used in Equation (3), specifically, their second term is $\nu^{1.2}$ for pure ice (Matzler, 1998). Perry and Straiton

(1973) obtained values of ε' and ε'' from measurements at $-28\,°$C. Mishima *et al*. (1983) measured the absorption spectrum from 8 to 25 cm^{-1} (400–1250-μm wavelength or 240–750 GHz) for single crystals of ice at four temperatures (80, 100, 150, 202 K). The plotted values of the imaginary dielectric constant ε'' are estimated from their measurements of n'' at 202 K and assuming $\varepsilon' = 3.15$. Whalley and Labbe (1969) measured the absorption spectrum from 17 to 42 cm^{-1} (238–588-μm wavelength or 510–1260 GHz) for blocks of ice at 100 and 200 K. We converted their measured values of n'' to ε'' also assuming $\varepsilon' = 3.15$. Berte *et al*. (1969) made measurements for thin films of ice ($<$1-μm thick) at 100 K from 100 to 8000 cm^{-1} (or 3000GHz to 240 THz). The plotted ε'' are taken from their Table III. They also presented some 'preliminary and not very accurate' measurements of a 1-mm thick sample for 30 to 60 cm^{-1} (900–1800 GHz) and estimated the value at 80 cm^{-1} (2400 GHz).

In comparisons with the above laboratory data, we found the differences between the modified LH model results and the measurements is generally less than $\sim$12% for frequencies $<$800 GHz and about 15 to 40% at frequencies⩾3000 GHz. In the frequency range of 900 to 2400 GHz, the only available data are the preliminary measurements by Berte *et al*. (1969), which may have large errors as stated in their paper. Also, we note that because of difficulties in accurately measuring ε'' of ice over the low frequency range (1–100 GHz) due to its low magnitude, large discrepancies still exist among other data sets derived from different experimental techniques. For example, Koh (1997)'s results obtained using an interference technique at 75 to 110 GHz were a factor of $\sim$3 lower than those of *Mätzler and Wegmüller*'s. Until additional experimental data become available, however, the modified LH model can be used to bridge the gaps between various data sets.
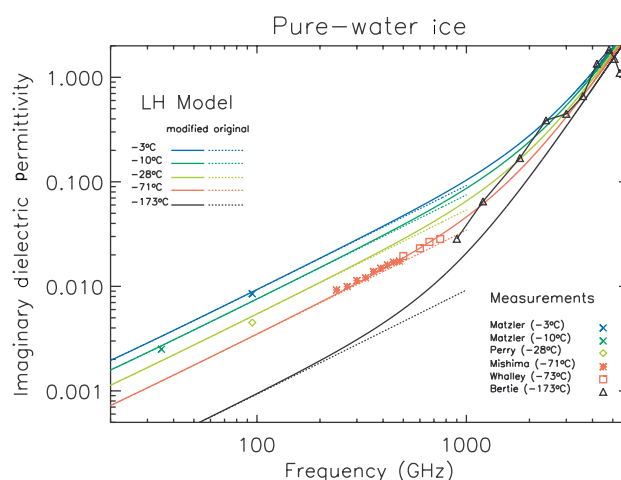
Figure 1. Computed and measured imaginary part of ice dielectric permittivity. The solid lines are ε'' computed using the modified LH formula (5), the dotted lines are those computed using the original LH formula (3)

The measured values for the real part of ice permittivity ε' are shown in Figure 2. The data labeled 'from Ulaby' are taken from Ulaby *et al.* (1981), which consisted of a set of measurements by Cumming (1952); Hippel (1954); Vant *et al.* (1974); Lamb (1946); Lamb and Turney, 1949; Perry and Straiton, 1973. Other data are from Bertie *et al.*, 1969.

The measurements of real permittivity of ice remain fairly constant over the broad microwave spectrum. Differences between the various measured data and the LH model value of 3.15 (shown as the straight line in Figure 2) are generally less than 5% at frequencies <1000 GHz. At higher frequencies (>1000 GHz), the differences increase slightly but remain <15% in general.

3.2. The permittivity for pure liquid water

For liquid water, the measured real and imaginary parts of dielectric permittivity are shown in Figure 2 and Figure 3 respectively. Measurements by Lowan (1949), Klein and Swift (1977) were at frequencies mainly below 120 GHz, while the data from Liebe *et al.* (1991) are in the range from 5 to 410 GHz for temperatures $\leqslant 20\,°C$.

The differences between measurements and the LH model are generally less than ~5%. However, few measurements are made below 0 °C. Values of the dielectric permittivity of super-cooled pure liquid water (<0 °C) are mostly computed from models (e.g. Ulaby *et al.*, 1981, (p2020−2025); Hulst, 1981, (p281−284)).

4. Sensitivity in microwave remote sensing applications

Cloud measurements using passive microwave instruments from space are relatively new and have important atmospheric applications. For example, recent observations with the limb-viewing MLS instrument
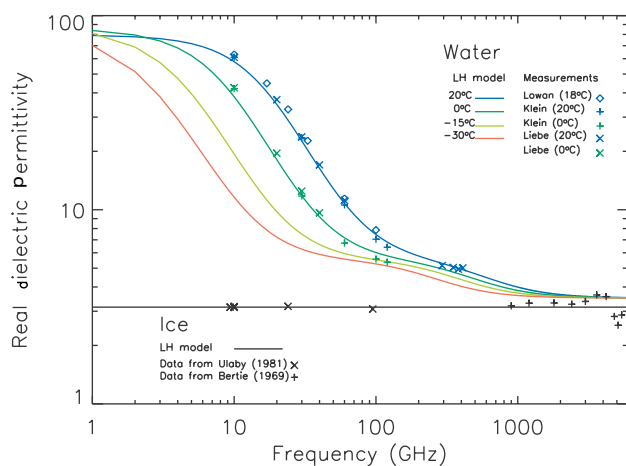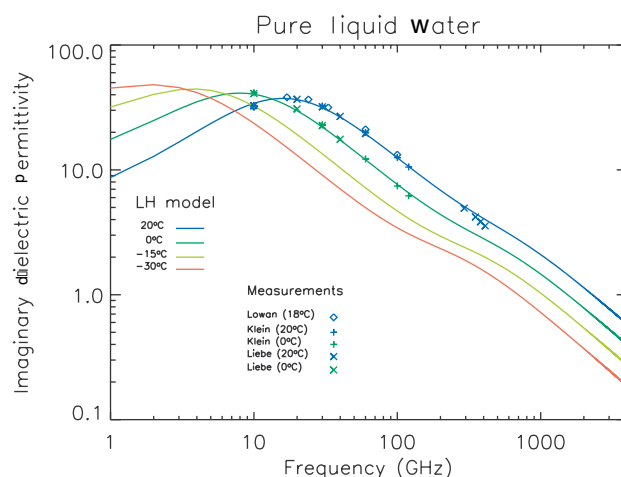
Figure 3. Computed and measured imaginary part of liquid water dielectric permittivities. The solid curves are ε' computed using the LH formula (4)

onboard the Upper Atmosphere Research Satellite (UARS) on cloud occurrence frequency and cloud ice content in the upper troposphere have important applications in research related to the convective scale perturbations in the tropical tropopause layer (TTL) and their potential influence on stratospheric dehydration (e.g. Jiang *et al.*, 2004; Read *et al.*, 2004; Wu *et al.*, in press).

Ice particles and water droplets have different Mie radiative properties in cold air conditions, mainly caused by their permittivity differences. Figure 4(a) shows the Mie extinction (solid lines) and scattering (dotted lines) efficiencies calculated at four selected MLS frequencies for ice particles (blue) and water droplets (red) at diameters between 1 and 4000 microns. The complex permittivities for ice and liquid water are computed for typical mid- to upper-tropospheric temperatures of −60 °C and −15 °C, respectively. From this example, we see that the Mie extinction and scattering efficiencies of small liquid water particles (diameter < 500 µm) are much higher than those of small ice particles. Most importantly, for these ice particles, which account for most cloud ice content in the upper troposphere, scattering occurs nearly in the Rayleigh regime at the MLS frequencies. In other words, for most upper-tropospheric clouds, the Mie coefficient increases with ice particle size.

The Mie phase function depends mainly on the particle size parameter $(\chi = 2\pi r/\lambda)$, but it is also influenced by the complex permittivity. Figure 4(b) illustrates the computed phase functions for single ice particles and water droplets with various particle size parameters. The dielectric permittivity values are computed for ice or water at 203 GHz using the same temperatures as in Figure 4(a). The single scattering albedo (ω_0) shown for each particle size is the ratio of Mie scattering to extinction efficiencies. For small size parameter (e.g. $\chi < 0.1$), both ice and water scatter radiation in nearly equal quantities forwards and backwards and the single scattering albedo is small.

Figure 2. Computed and measured real part of ice and water dielectric permittivity. The solid curves are ε' computed using the LH formula (3) for ice and (4) for liquid water
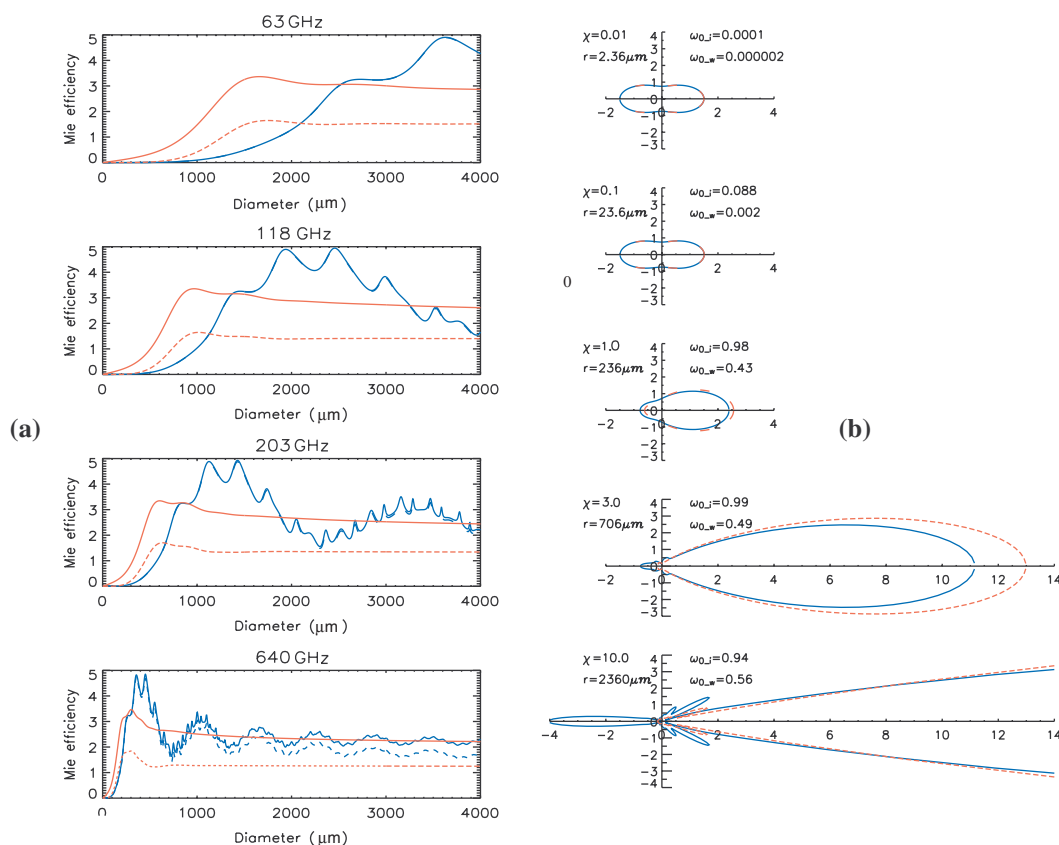
Figure 4. (a) Mie extinction (solid line) and scattering (dotted line) efficiencies for ice (blue) and liquid water (red). (b) Phase function for single ice particles (solid line) and water droplet (dotted line) with different size parameters. The complex dielectric permittivities are computed at $-60\,^{\circ}$C for ice and $-15\,^{\circ}$C for liquid water

For large size parameter (e.g. $\chi > 1$), the radiation is heavily concentrated in a narrow forward lobe, the single scattering albedo increases, and the ice and water phase functions become different. At very large size parameter (e.g. $\chi = 10$), the backward scattering of ice particles is much larger than that of liquid droplets. Also notably, the single scattering albedo of ice (ω_{0_i}) is much larger than that of water (ω_{0_w}) for all particle sizes, mainly due to the difference in Mie efficiencies.

In practice, we have found ice particles with diameters of $\sim$100 to 300 µm produce the strongest signatures in UARS MLS radiances (Wu *et al.*, in press). Scattering by such particles occurs in the Rayleigh regime for MLS frequencies $\leqslant$640 GHz. From our calculations summarized in Table I, a 20% uncertainty in the imaginary part of permittivity for an ice particle in that size range will result in $\sim$1 to 10% errors in both the Mie extinction coefficients and the single scattering albedos at typical MLS measurement frequencies. For 640 GHz, the error is about 1% or less, which could be the best for the cloud measurement in the TTL (Wu and Jiang, 2004). Similar uncertainties in the real part of permittivity will result in larger errors, e.g. a 5% uncertainty will result in $\sim$1 to 10% error in typical MLS frequencies. Fortunately, the measured value for the real part of ice permittivity is more certain at the MLS frequency range.

5. Summary

The empirical model of dielectric ice permittivity is extended to frequencies as high as 3000 GHz from the original LH formulae. The modified LH model may have uncertainties of about 12% in the imaginary part and of 5% in the real part of ice permittivity at a frequency range of 100 to 1000 GHz in comparisons with laboratory data. At higher frequencies ($>$1000 GHz), the uncertainties may be up to $\sim$50% in the imaginary part and $\sim$15% in the real part. For liquid water, uncertainties are 5% or less in both imaginary and real parts of the permittivity for temperature $\leqslant$0 $^{\circ}$C. Additional uncertainties may exist at lower temperatures where little laboratory measurements are available.

Such uncertainties in ice and water permittivity may result in about 10 to 20% in combined errors in the Mie theory calculations. Thus, more laboratory measurements are needed to improve our knowledge of permittivity. Also, our empirical model is based only on pure ice and liquid water. Impurity effects on ice permittivity are little known, such as those formed in polar stratospheric clouds (PSCs). Although this study is primarily motivated by the current MLS cloud studies, it also has important applications to other ground, airborne and space microwave sensors.

Table I. For each typical UARS and EOS MLS radiometer frequency, this table lists the Mie extinction coefficient (ξ_e), single scattering albedo (ω_0) for a typical ice particle of 200-μm diameter at three different temperatures ($-15\,°C$, $-30\,°C$ and $-60\,°C$) and their percentage errors resulting from a 20% uncertainty in the imaginary part of ice permittivity or a 5% uncertainty in the real part of ice permittivity

Typical MLS radiometers	T (°C)	ε'	ε''	ξ_e	$\lvert\Delta\xi_{el}\rvert(\Delta\varepsilon' = 5\%)$	$\lvert\Delta\xi_e/\xi_e\rvert$ ($\Delta\varepsilon' = 5\%$)(%)	$\lvert\Delta\xi_{el}\rvert(\Delta\varepsilon'' = 20\%)$	$\lvert\Delta\xi_e/\xi_e\rvert$ ($\Delta\varepsilon'' = 20\%$)(%)	ω_0	$\lvert\Delta\omega_0\rvert$ ($\Delta\varepsilon' = 5\%$)	$\lvert\Delta\omega_0/\omega_0\rvert$ ($\Delta\varepsilon' = 5\%$)(%)	$\lvert\Delta\omega_0\rvert$ ($\Delta\varepsilon'' = 20\%$)	$\lvert\Delta\omega_0/\omega_0\rvert$ ($\Delta\varepsilon'' = 20\%$)(%)
63 GHz	−15		0.0042	0.000397	0.0000027	0.7	0.00005	12.9	0.356	0.033	9.3	0.041	11.4
	−30	3.15	0.0033	0.000342	0.0000005	0.1	0.00004	11.7	0.414	0.035	8.4	0.043	10.5
	−60		0.0024	0.000287	0.0000036	1.3	0.00003	10.1	0.493	0.035	7.1	0.045	9.2
118 GHz	−15		0.0079	0.00269	0.00010	3.7	0.0002	6.9	0.654	0.031	4.7	0.042	6.5
	−30	3.15	0.0062	0.00249	0.00011	4.5	0.0001	5.9	0.707	0.028	4.0	0.039	5.5
	−60		0.0045	0.00229	0.00012	5.3	0.0001	4.6	0.768	0.024	3.1	0.034	4.4
190 GHz	−15		0.0128	0.0147	0.00095	6.4	0.0005	3.5	0.822	0.019	2.4	0.028	3.4
	−30	3.15	0.0100	0.0142	0.00096	6.9	0.0004	2.9	0.855	0.016	1.9	0.024	2.8
	−60		0.0073	0.0136	0.00100	7.4	0.0003	2.2	0.890	0.013	1.4	0.019	2.2
203 GHz	−15		0.0137	0.0189	0.00127	6.7	0.0006	3.4	0.839	0.018	2.1	0.026	3.1
	−30	3.15	0.0107	0.0183	0.00131	7.2	0.0005	2.6	0.869	0.015	1.7	0.022	2.5
	−60		0.0078	0.0176	0.00134	7.6	0.0003	2.0	0.901	0.012	1.3	0.017	1.9
240 GHz	−15		0.0162	0.0359	0.00268	7.5	0.0009	2.5	0.875	0.014	1.6	0.021	2.4
	−30	3.15	0.0127	0.0350	0.00273	7.8	0.0007	2.0	0.899	0.011	1.3	0.018	2.0
	−60		0.0093	0.0340	0.00277	8.1	0.0005	1.5	0.924	0.009	1.0	0.014	1.5
640 GHz	−15		0.0458	1.413	0.19014	13.5	0.0101	0.7	0.945	0.004	0.4	0.010	1.1
	−30	3.15	0.0366	1.403	0.19027	13.6	0.0081	0.6	0.956	0.003	0.4	0.008	0.9
	−60		0.0274	1.392	0.19039	13.7	0.0061	0.4	0.967	0.002	0.2	0.006	0.7
2500 GHz	−15		0.4906	2.380	0.07139	3.0	0.0439	1.8	0.470	0.021	4.4	0.012	2.6
	−30	3.15	0.4544	2.353	0.08254	3.5	0.0448	1.9	0.481	0.022	4.8	0.016	3.3
	−60		0.4187	2.323	0.09618	4.1	0.0452	1.9	0.495	0.025	5.0	0.020	4.0

References

Bertie JE, Labbe HJ, Whalley E. 1969. Absorptivity of ice I in the range 4000-30 cm^{-1}. *Journal of Chemical Physics* **50**: 4501–4520.

Cumming WA. 1952. The dielectric properties of ice and snow at 3.2 centimeters. *Journal of Applied Physics* **23**: 768–773.

Hippel A von (ed.). 1954. *Dielectric Materials and Applications*. MIT Press: Cambridge, MA.

Hufford G. 1991. A model for the complex permittivity of ice at frequencies below 1 THz. *International Journal of Infrared Millimeter Waves* **12**: 677–682.

Jiang JH, Wang B, Goya K, Hocke K, Eckerman SD, Ma J, Wu DL, Read WG. 2004. Geographical distribution and inter-seasonal variability of tropical deep convection: UARS MLS observations and analyses. *Journal of Geophysical Research* **109**: pgsD3, D03111, 10.1029/2003JD003756.

Klein LA, Swift CT. 1977. An improved model for the dielectric constant of sea water at microwave frequencies. *IEEE Transactions on Antennas and Propagation* **25**: 104–111.

Koh G. 1997. Dielectric properties of ice at millimeter wavelengths. *Geophysical Research Letters* **24**: 2311–2313.

Lamb J. 1946. Measurements of the dielectric properties of ice. *Discuss Faraday Society* **42A**: 238.

Lamb J, Turney A. 1949. The dielectric properties of ice at 1.25 cm. wavelength. *Proceedings of the Physical Society of London Section B* **62**: 272–273.

Liebe HJ, Hufford GA, Manabe T. 1991. A model for the complex permittivity of water at frequencies below 1 THz. *International Journal of Infrared and Millimeter Waves* **12**(7): 659–674.

Liebe HJ, Manabe T, Hufford GA. 1989. Millimeter-wave attenuation and delay rates due to fog/cloud conditions. *IEEE Transactions on Antennas and Propagation* **37**: 1617–1623.

Lowan AN. 1949. Tables of scattering functions for spherical particles, U.S. National Bureau of Standards. *Applied Mathematics Series 4*. United States Government Printing Office: Washington, DC.

Mätzler C. 1998. Microwave properties of ice and snow. In *Solar System Ices*, Schmitt B et al (eds). Kluwer Academic Publishers: Dordrecht; 241–257.

Mätzler C, Wegmüller U. 1987. Dielectric properties of freshwater ice at microwave frequencies. *Journal of Physics D: Applied Physics* **20**: 1623–1630.

Mishima O, Klug DD, Wahlley E. 1983. The far-infrared spectrum of ice Ih in the range 8-25cm^{-1}. Sound waves and difference bands, with application to Saturn's rings. *Journal of Chemical Physics* **78**: 6399–6404.

Perry J, Straiton AW. 1973. Revision of dielectric-constant of ice in millimeter-wave spectrum. *Journal of Applied Physics* **44**(11): 5180–5180.

Read WG, Wu DL, Waters JW, Pumphrey HC. 2004. Dehydration in the tropical tropopause layer: implications from UARS MLS. *Journal of Geophysical Research* **109**: D6, D06110, 10.1029/2003JD004056.

Ulaby FT, Moore RK, Fung AK. 1981. *Microwave Remote Sensing: Active and Passive, Volume I: Microwave Remote Sensing Fundamentals and Radiometry*. Addison-Wesley Publishing Company/Don Mills.

Vant MR, Gray, RB, Ramseier RO, Makios, V. 1974. Dielectric properties of fresh and sea ice at 10 and 35 GHz. *Journal of Applied Physics* **45**: 4712.

von de Hulst HC (ed.). 1981. *Light Scattering by Small Particles*. Dover: New York; 470.

Whalley E, Labbe, HJ. 1969. Optical spectra of orientationally disordered crystals. III. Infrared spectra of the sound waves. *Journal of Chemical Physics* **51**: 3120–3127.

Wu DL, Jiang JH. 2004. EOS MLS algorithm theoretical basis for cloud measurements, Technical Report, Jet Propulsion Laboratory, *D-19 299/CL#04-2160, EOS MLS DRL 601(part 6), ATBD-MLS-06*. (For additional information visit http://mls.jpl.nasa.gov/jonathan/cloud_ice/).

Wu DL, Read WG, Dessler AE, Sherwood SC, Jiang JH. In press. UARS MLS cloud ice measurements and implications for H2O transport near the tropopause. *Journal of Atmospheric Science*.